

000
001
002
003
004
005
006
007
008
009
010
011054
055
056
057
058
059
060
061
062
063
064
065
066
067
068
069
070
071
072
073
074
075
076
077
078
079
080
081

Abstract

The ABSTRACT is to be in fully-justified italicized text, at the top of the left-hand column, below the author and affiliation information. Use the word “Abstract” as the title, in 12-point Times, boldface type, centered relative to the column, initially capitalized. The abstract is to be in 10-point, single-spaced type. Leave two blank lines after the Abstract, then begin the main text. Look at previous CVPR abstracts to get a feel for style and length.

1. Introduction

1.1. Introduction

Estimating depth from images is an important open problem with applications to robotics, autonomous driving, and medical imaging. Dense depth maps are useful precursors to higher-level scene understanding tasks such as pose estimation and object detection.

However, traditional approaches to depth estimation, such as stereo, suffer from lower performance when confronted with small angles or faraway objects. More exotic approaches use FMCW or time-of-flight LiDAR technologies, but these approaches are currently expensive and bulky.

The most promising solution to these issues uses deep learning and convolutional neural networks to perform *monocular depth estimation*, estimating dense depth maps from single RGB images. However, this problem is under-constrained due to *inherent scale ambiguity*, the unresolvable tradeoff between size and distance in single images. In practice, this issue commonly manifests itself in many monocular depth networks, and indeed, Wonka et. al. (cite) showed that if the method has oracle access to the ground truth median depth, then correcting the output of the CNN to match this median depth produces better depth maps both qualitatively and quantitatively.

In this paper, we go further and show that by augmenting the RGB image with a histogram of global image depths, we can achieve substantially improved performance (and gen-

Anonymous CVPR submission

Paper ID ****

eralizability) over state-of-the-art monocular depth estimators. By performing an exact, weighted histogram matching on the output depth map of the depth estimator, we can match the depth histogram of the scene to the depth histogram of our estimate. This histogram matching is described in (cite) and is flexible enough to accommodate different pixel reflectances in the RGB image. Finally, this histogram can be captured relatively inexpensively using only a single pixel single-photon avalanche diode (SPAD) and pulsed laser illumination diffused over the field of view, representing a significant improvement in cost and simplicity over multi-pixel LiDAR arrays with expensive scanning mechanisms. It is worth noting that SPADs of this type have already made their way into existing smartphones, such as the iPhone X, and will likely play a role in future mobile sensing platforms as well.

Our method is not without limitations. It still requires a laser and single-pixel LiDAR detector, and as such, is sensitive to ambient photons. Being a variant of histogram matching, our method is unable to transpose the values of pixels (i.e. if pixel a is farther than pixel b in the input, it will be farther than pixel b in the output). In other words, our method is not able to resolve ordinal depth errors (errors where an object is wrongly placed closer or farther relative to another object). Finally, our method is non-differentiable, and is therefore unsuitable for end-to-end optimization of multi-part networks.

- We introduce the idea of augmenting an RGB camera with a global depth histogram to address scale ambiguity error in monocular depth estimators.
- We analyze our approach on indoor scenes using the NYU Depth v2 dataset. We demonstrate that our approach is able to resolve scale ambiguity while being fast and easy to implement.
- We build a hardware prototype and evaluate the efficacy of our approach on real-world data, assessing both the quality and the ability of our method to help generalization of monocular depth estimators across scene types.

108

2. Related Work

109

110

111

112

113

114

115

116

117

118

119

120

121

122

123

124

125

126

127

128

129

130

131

132

133

134

135

136

137

138

139

140

141

142

143

144

145

146

147

148

149

150

151

152

153

154

155

156

157

158

159

160

161

162

163

164

165

166

167

168

169

170

171

172

173

174

175

176

177

178

179

180

181

182

183

184

185

186

187

188

189

190

191

192

193

194

195

196

197

198

199

200

201

202

203

204

205

206

207

208

209

210

211

212

213

214

215

et. al [16] provide a simple and concise method that also achieves an exact histogram match while being very fast. In the image reconstruction space, Swoboda and Schnörr [20] use a histogram to form an image prior based on the Wasserstein distance for image denoising and inpainting. Rother et. al. [1] use a histogram prior to create an energy function that penalizes foreground segmentations with dissimilar histograms. In a slightly different vein, Zhang et. al. [24] train a neural network to produce realistically colorized images given only a black-and-white image and a histogram of global color information.

Our method is essentially a modified form of the algorithm in [16], modified for our particular use case. Also worth noting is the fact that most algorithms compute histograms from existing images, whereas our method measures the depth histogram indirectly using photon arrivals.

3. Method

In this section, we describe the measurement model for a single-pixel time-of-flight lidar sensor under diffuse, pulsed laser illumination.

3.1. Measurement Model

Consider a laser which emits a pulse at time $t = 0$ with time-varying intensity $g(t)$ uniformly illuminating some 3D scene. We parameterize the geometry of the scene as a height map $z(x, y)$. Neglecting albedo and falloff effects, an ideal detector counting photon events from a location (x, y) in the time interval $(n\Delta t, (n + 1)\Delta t)$ would record

$$\lambda_{x,y}[n] = \int_{n\Delta t}^{(n+1)\Delta t} (f * g)(t - 2z(x, y)/c) dt \quad (1)$$

where c is the speed of light, and f is a function that models the temporal uncertainty in the detector. Single-photon avalanche diodes (SPADs) are highly sensitive photodetectors which are able to record single photon events with high temporal precision [?]. Since the event corresponding to the detection of a photon can be described with a Bernoulli random variable, the total number of accumulated photons in this time interval follows a Poisson distribution according to

$$h[n] \sim \mathcal{P} \left(\sum_{x,y} \alpha_{x,y} \eta \lambda_{x,y}[n] + b \right) \quad (2)$$

where $\alpha_{x,y} = r_{x,y}/z(x, y)^2$ captures the attenuation of the photon counts due to the reflectance $r(x, y)$ of the scene and due to the inverse square falloff $1/z(x, y)^2$. In addition, η is the detection probability of a photon triggering a SPAD event, and $b = \eta a + d$ is the average number of background

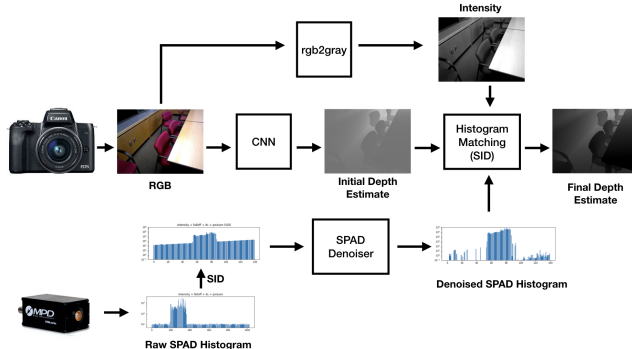


Figure 1: **Overview of the full pipeline** We use a CNN to get an initial per-pixel depth estimate. Then we perform exact histogram matching using intensity-weighted pixel values on the corrected SPAD data.

detections resulting from ambient photons a and erroneous “dark count” events d resulting from noise within the SPAD.

3.2. Monocular depth estimation with global depth hints

Given a single RGB image $I(x, y)$ and a vector of photon arrivals $h[n]$ described by equation 2, we seek to reconstruct the ground truth depth map $z(x, y)$. Our method has two parts. First, we **initialize** our estimate of the depth map from the single RGB image via a monocular depth estimator described below. Second, we **refine** this depth map using the captured measurements $h[n]$ via exact histogram matching.

Initialization The first step in our method is to produce an initial estimate of ground truth depth. Convolutional Neural Networks have been shown to produce accurate, if poorly-scaled, estimates of depth from only a single image. We therefore choose to initialize our depth map estimate $\hat{z}^{(0)}(x, y)$ using a CNN. However, any depth estimator reliant on only a single view may be used for this step. Furthermore, in the larger context of our algorithm, it is more important that the network predict the correct ordinal relationships between pixels - that is, to predict the correct relative ordering of pixels a and b , rather than to get all pixels exactly correct.

Exact Histogram Matching An image’s *histogram* is a pair of vectors (h, b) where h_i is the number of pixels of the image whose value lies in the range $[b_i, b_i + 1]$. Then, given a source image S with histogram (h_s, b) and a target histogram (h_t, b) , histogram matching generates a new image M such that $h_m \approx h_t$ and the pixel values in M are in the same relative order as in S . The full details of the exact histogram matching algorithm can be found in [16].

However, for our purposes, we need to modify our algorithm to accommodate differing per-pixel weights. We can account for squared depth falloff

SPAD Denoising

- Talk about histogram matching in the ideal case, jump straight to intensity
- Talk about histogram matching in our case, and how it approaches the ideal case. Discuss the following corrections
 - Ambient/DC - Use [?] to justify looking for large edges, then the ambient estimate to get rid of the noise floor.
 - Falloff
- Talk about how the histogram matching works with intensity considerations applied, briefly.
- We don’t address jitter or poisson noise.

$$h[n] \sim \mathcal{P} \left(\sum_{x,y} \alpha_{x,y} \eta \lambda_{x,y}[n] + b \right) \quad (3)$$

Given a SPAD with histogram h according to the above equation, we first process the SPAD to remove the effects of some of the terms. First, we

3.3. Implementation Details

For the Monocular Depth Estimator, we use pretrained versions of the the Deep Ordinal Regression Network (DORN) [] and the DenseDepth Network. The exact histogram matching method is as described in [].

4. Simulation

4.1. Implementation Details

- Number of bins used, depth range, laser parameters, use of intensity image.
- Using

NYU Depth v2 The NYU Depth v2 Dataset consists of 249 training and 215 testing scenes of RGB-D data captured using a Microsoft Kinect. We used a version of DORN pre-trained according to [6] as our CNN.

324

5. Hardware Prototype

325

5.1. Setup

326

- Description of hardware used
- Images of scenes used

327

6. Discussion

328

References

329

330

331

332

333

334

335

336

337

338

339

340

341

342

343

344

345

346

347

348

349

350

351

352

353

354

355

356

357

358

359

360

361

362

363

364

365

366

367

368

369

370

371

372

373

374

375

376

377

- [1] *Cosegmentation of image pairs by histogram matching incorporating a global constraint into mrfs*, volume 2006 IEEE Computer Society Conference on Computer Vision and Pattern Recognition (CVPR’06) 1. IEEE, 2006.
- [2] *Depth map prediction from a single image using a multi-scale deep network*, volume Advances in neural information processing systems, 2014.
- [3] *Deeper depth prediction with fully convolutional residual networks*, volume 2016 Fourth international conference on 3D vision (3DV). IEEE, 2016.
- [4] *Multi-scale continuous crfs as sequential deep networks for monocular depth estimation*, volume Proceedings of the IEEE Conference on Computer Vision and Pattern Recognition, 2017.
- [5] *Unsupervised monocular depth estimation with left-right consistency*, volume Proceedings of the IEEE Conference on Computer Vision and Pattern Recognition, 2017.
- [6] *Deep ordinal regression network for monocular depth estimation*, volume Proceedings of the IEEE Conference on Computer Vision and Pattern Recognition, 2018.
- [7] *Detail Preserving Depth Estimation from a Single Image Using Attention Guided Networks*, volume 2018 International Conference on 3D Vision (3DV). IEEE, 2018.
- [8] *Structured attention guided convolutional neural fields for monocular depth estimation*, volume Proceedings of the IEEE Conference on Computer Vision and Pattern Recognition, 2018.
- [9] Ibraheem Alhashim and Peter Wonka. High quality monocular depth estimation via transfer learning. *arXiv*, page 1812.11941v2, 2018.
- [10] Rafael C Gonzalez and Richard E Woods. *Digital Image Processing*. 2008.
- [11] Derek Hoiem, Alexei A Efros, and Martial Hebert. Automatic photo pop-up. *ACM transactions on graphics(TOG)*:577–584, 2005.
- [12] Radu Horaud, Miles Hansard, Georgios Evangelidis, and Clément Ménier. An overview of depth cameras and range scanners based on time-of-flight technologies. *Machine vision and applications*, 27(7):1005–1020, 2016.
- [13] K Karsch, C Liu, and SB Kang. Depth transfer: Depth extraction from video using non-parametric sampling. *IEEE Trans Pattern Anal Mach Intell*, 36(11):2144–2158, 2014.
- [14] Robert Lamb and Gerald Buller. Single-pixel imaging using 3d scanning time-of-flight photon counting. *SPIE Newsroom*, 2010.

- [15] David B. Lindell, Matthew O’Toole, and Gordon Wetzstein. Single-photon 3d imaging with deep sensor fusion. *ACM Trans. Graph.*, page 1812.11941v2, 2018.
- [16] Jan Morovic, Julian Shaw, and Pei-Li Sun. A fast, non-iterative and exact histogram matching algorithm. *Pattern Recognition Letters*, 23(1-3):127–135, 2002.
- [17] C. Niclass, A. Rochas, P.-A. Besse, and E. Charbon. Design and characterization of a cmos 3-d image sensor based on single photon avalanche diodes. *IEEE Journal of Solid-State Circuits*, 40(9):1847–1854, 2005.
- [18] Mila Nikolova, You-Wei Wen, and Raymond Chan. Exact histogram specification for digital images using a variational approach. *Journal of Mathematical Imaging and Vision J Math Imaging Vis*, 46(3):309–325, 2013.
- [19] David Stoppa, Lucio Pancheri, Mauro Scanduzzo, Lorenzo Gonzo, Gian-Franco Dalla Betta, and Andrea Simoni. A cmos 3-d imager based on single photon avalanche diode. *IEEE Transactions on Circuits and Systems I: Regular Papers*, 54(1):4–12, 2007.
- [20] Paul Swoboda and Christoph Schnörr. Convex variational image restoration with histogram priors. *SIAM Journal of Imaging Sciences*, 6(3):1719–1735, 2013.
- [21] Chockalingam Veerappan, Justin Richardson, Richard Walker, Day-Uey Li, Matthew W Fishburn, Yuki Maruyama, David Stoppa, Fausto Borghetti, Marek Gersbach, and Robert K Henderson. A 160×128 single-photon image sensor with on-pixel 55ps 10b time-to-digital converter. 2011 IEEE International Solid-State Circuits Conference:312–314, 2011.
- [22] Y. Weiss, B. Schölkopf, and J. C. Platt, editors. *Learning depth from single monocular images*, volume Advances in neural information processing systems. MIT Press, 2006.
- [23] C Zhang, S Lindner, IM Antolovic, M Wolf, and E Charbon. A cmos spad imager with collision detection and 128 dynamically reallocating tdcs for single-photon counting and 3d time-of-flight imaging. *Sensors (Basel)*, 18(11), 2018.
- [24] Richard Zhang, Jun-Yan Zhu, Phillip Isola, Xinyang Geng, Angela S Lin, Tianhe Yu, and Alexei A Efros. Real-time user-guided image colorization with learned deep priors. *ACM Transactions on Graphics (TOG)*, 9(4), 2017.

	$\delta^1 \uparrow$	$\delta^2 \uparrow$	$\delta^3 \uparrow$	$rel \downarrow$	$rmse \downarrow$	$log10 \downarrow$
DORN	0.846	0.954	0.983	0.120	0.501	0.053
DORN + median rescaling	0.871	0.964	0.988	0.111	0.473	0.048
DORN + GT histogram matching	0.906	0.972	0.990	0.095	0.419	0.040
Proposed (SBR=10)	<u>0.903</u>	0.970	<u>0.989</u>	0.091	0.422	<u>0.040</u>
Proposed (SBR=50)	0.906	<u>0.971</u>	0.990	0.089	<u>0.410</u>	0.039
Proposed (SBR=100)	0.906	<u>0.971</u>	0.990	<u>0.090</u>	0.408	0.039
DenseDepth	0.847	0.973	0.994	0.123	0.461	0.053
DenseDepth + median rescaling	0.888	0.978	0.995	0.106	0.409	0.045
DenseDepth + GT histogram matching	0.930	0.984	0.995	0.079	0.338	0.034
Proposed (SBR=10)	0.922	0.982	<u>0.994</u>	0.082	0.361	0.036
Proposed (SBR=50)	0.925	<u>0.983</u>	0.995	<u>0.081</u>	0.348	<u>0.035</u>
Proposed (SBR=100)	0.926	0.983	0.995	<u>0.081</u>	0.346	0.035

Table 1: Simulated Results on NYU Depth v2. Bold indicates best performance for that metric, while underline indicates second best. The proposed scheme outperforms DenseDepth and DORN on all metrics, and even outperforms the median rescaling scheme, which has access to the true median depth value.

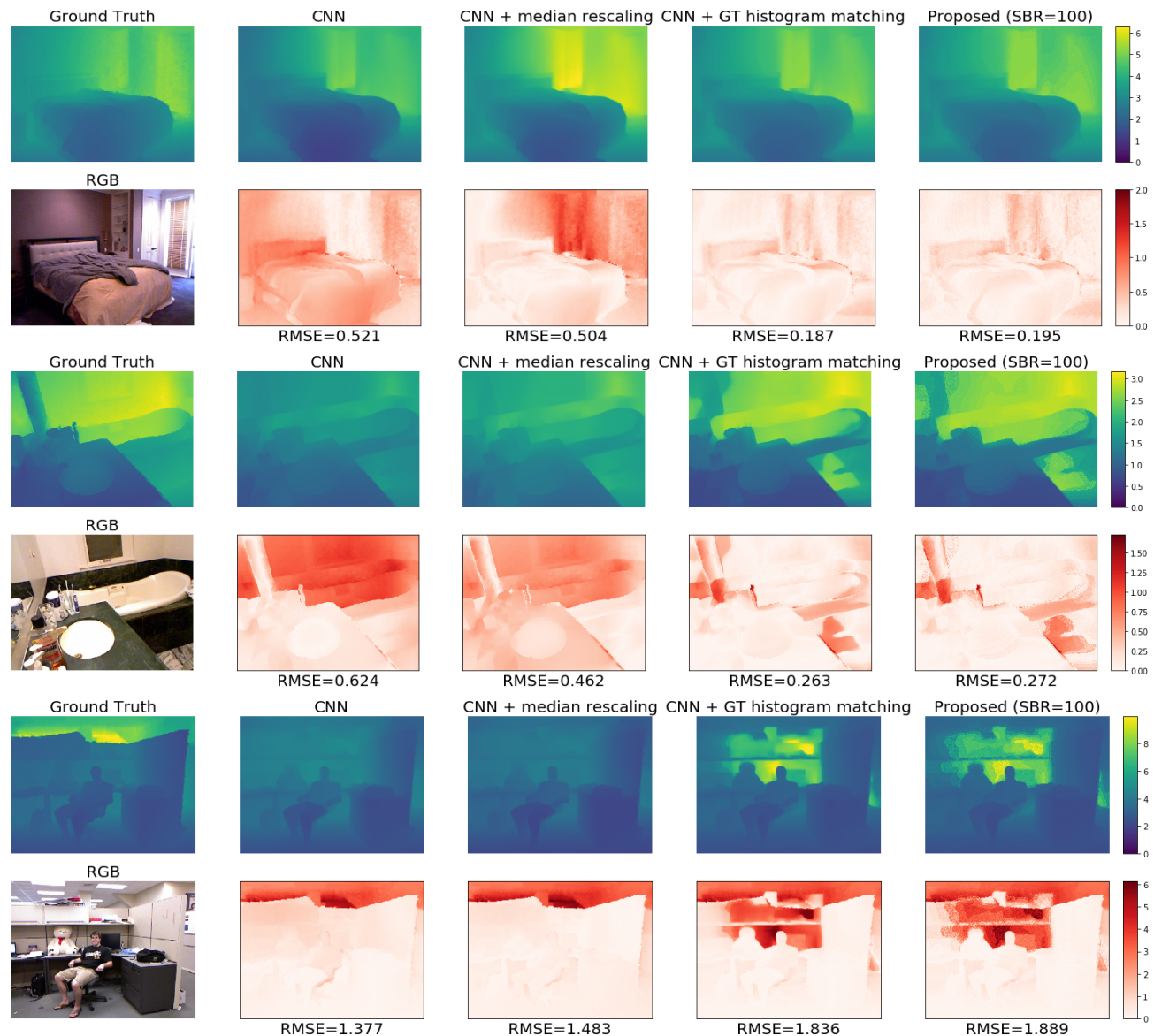


Figure 2: Selected Results on DenseDepth. First two examples demonstrate capability of proposed method to correct initial scaling/translation errors. Last example shows potential pitfall when ordinal depth is predicted incorrectly.

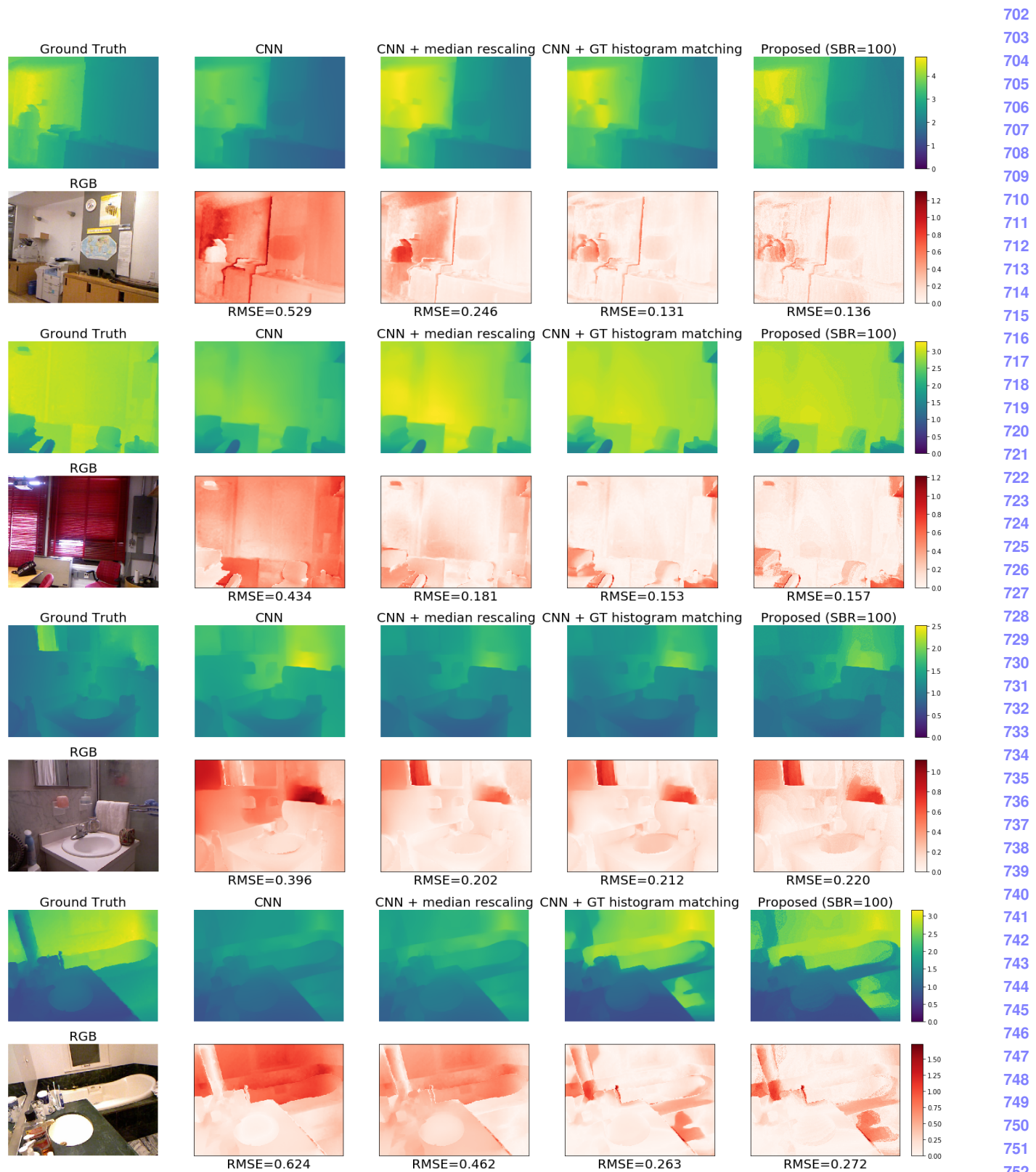


Figure 3: Results on DenseDepth

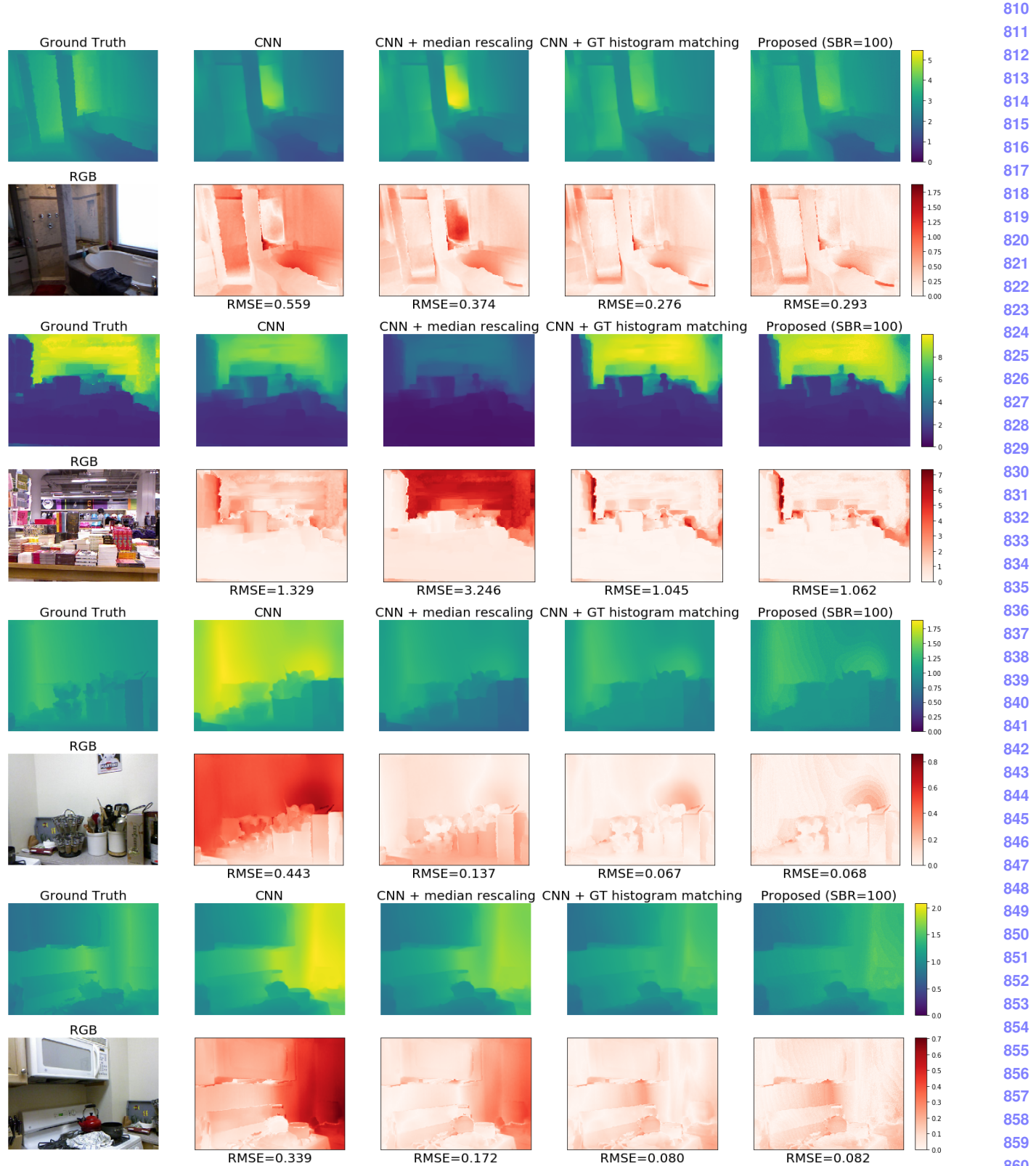


Figure 4: Results on DenseDepth

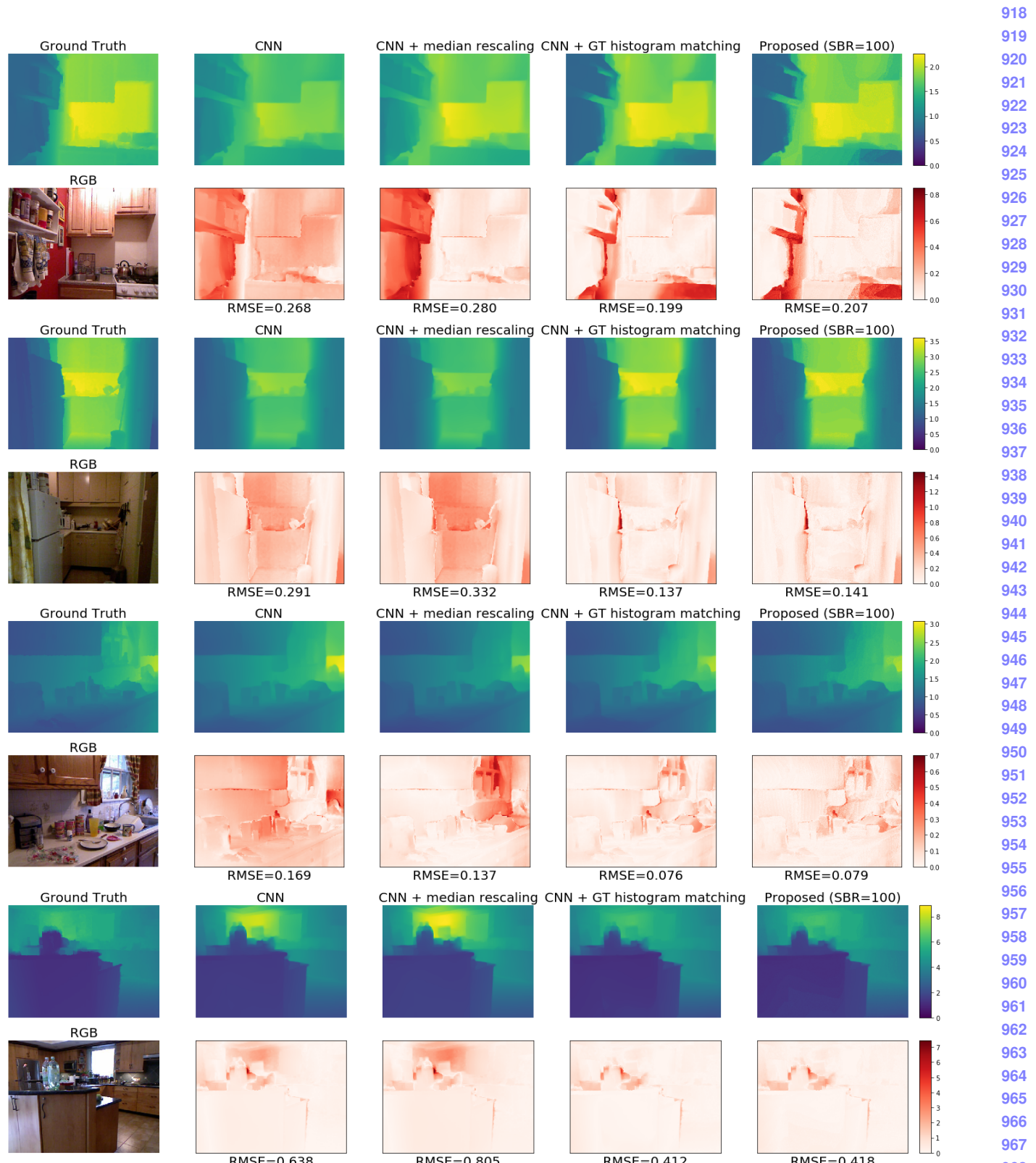


Figure 5: Results on DenseDepth

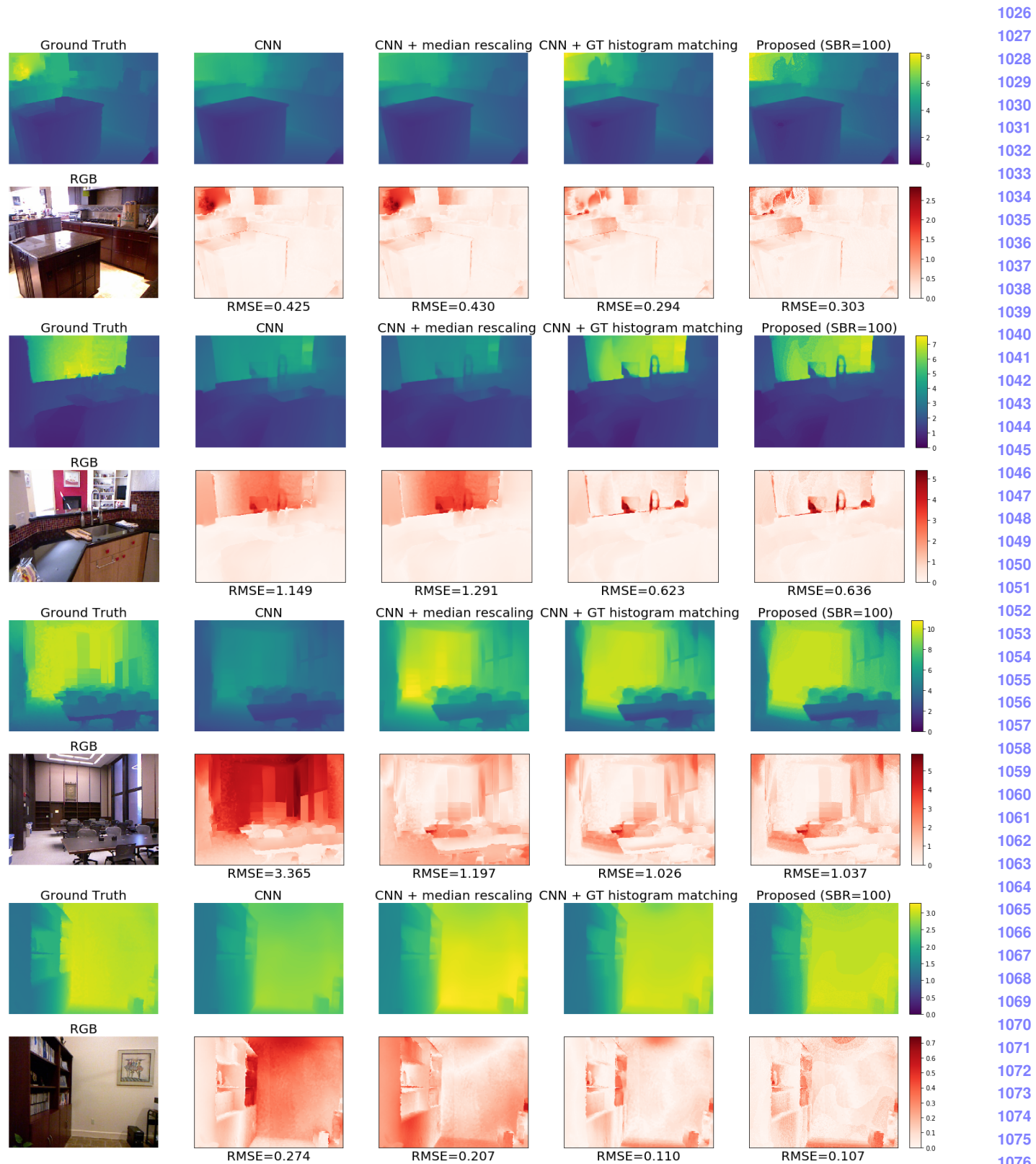


Figure 6: Results on DenseDepth

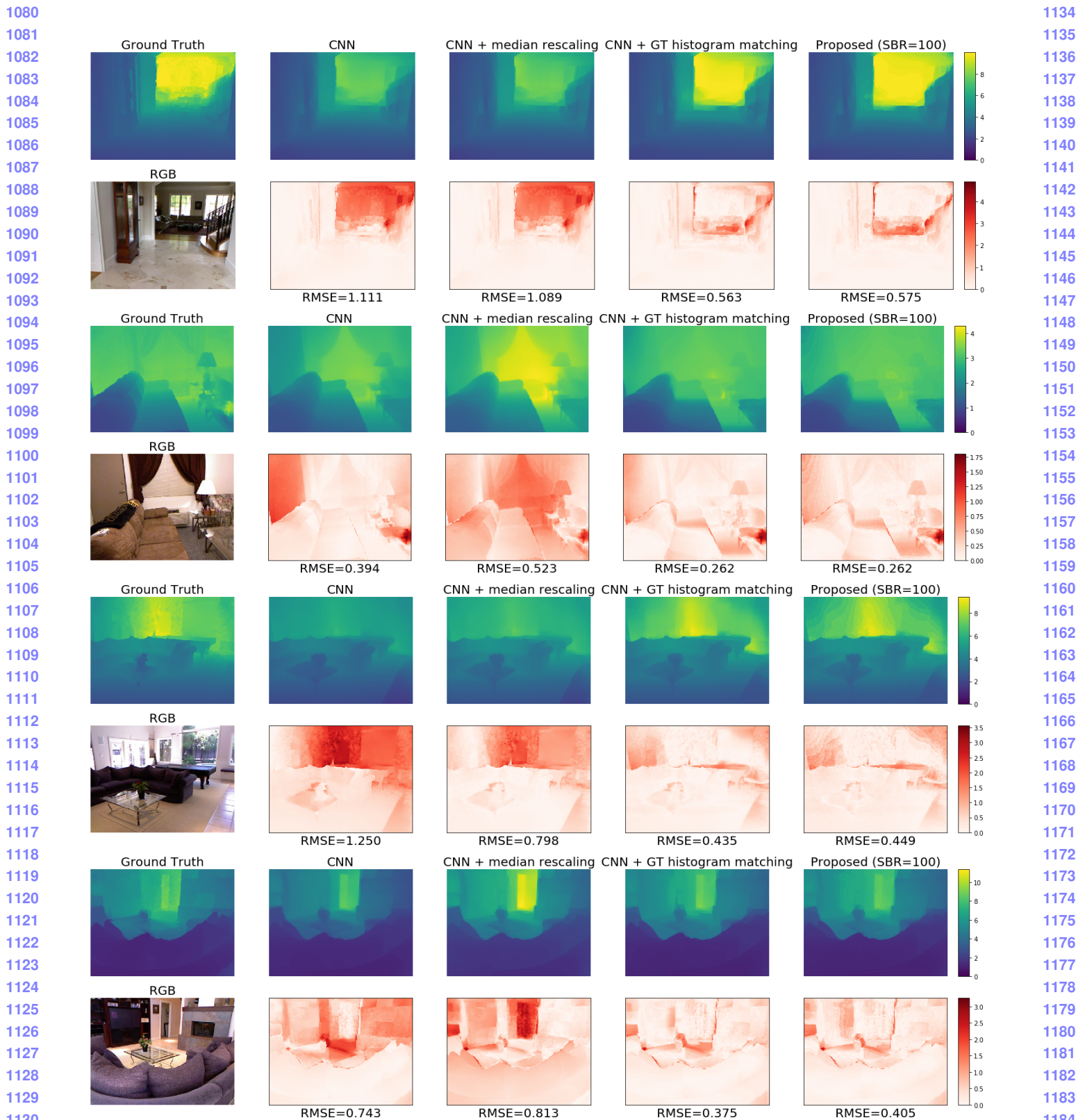


Figure 7: Results on DenseDepth

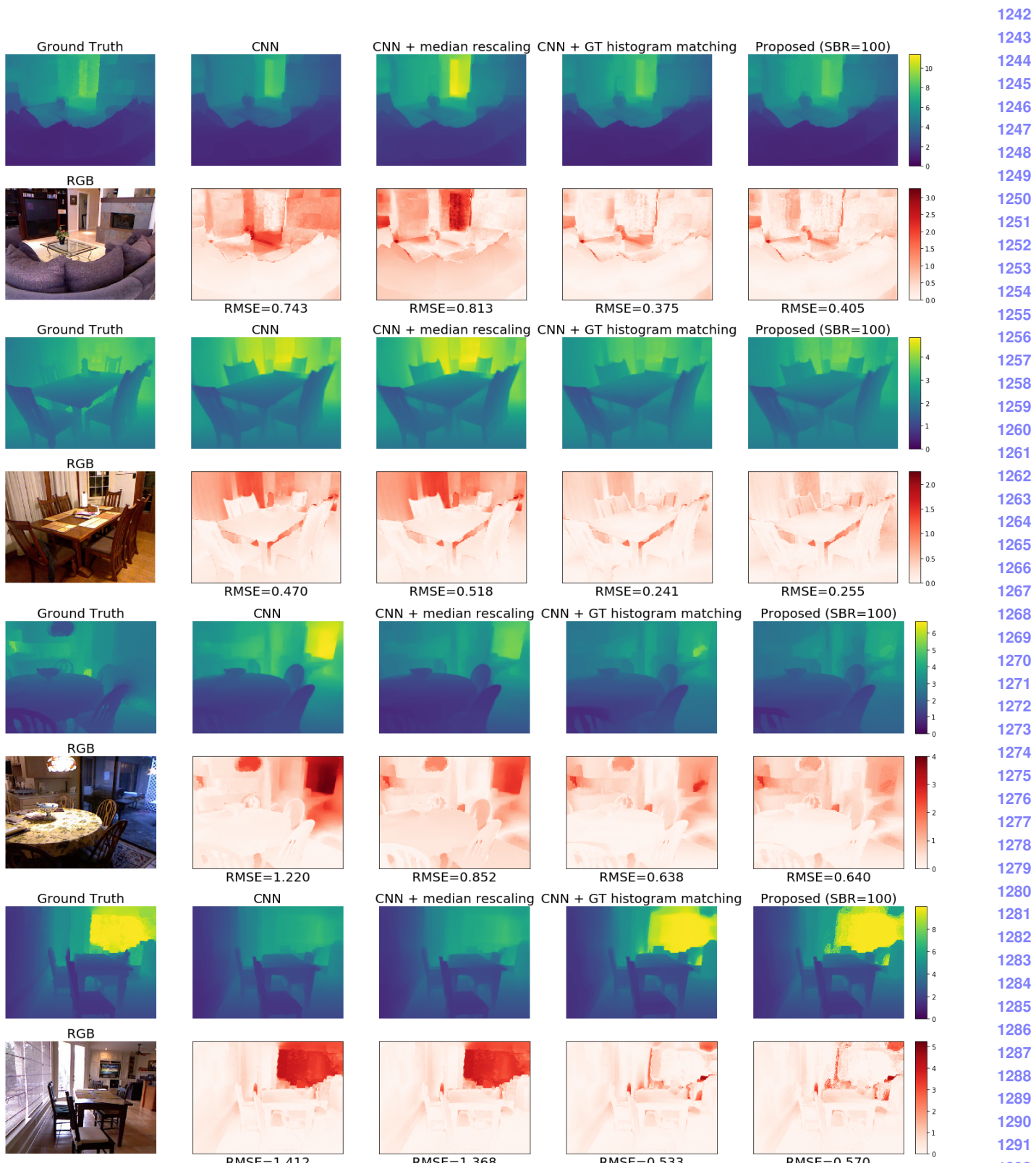


Figure 8: Results on DenseDepth

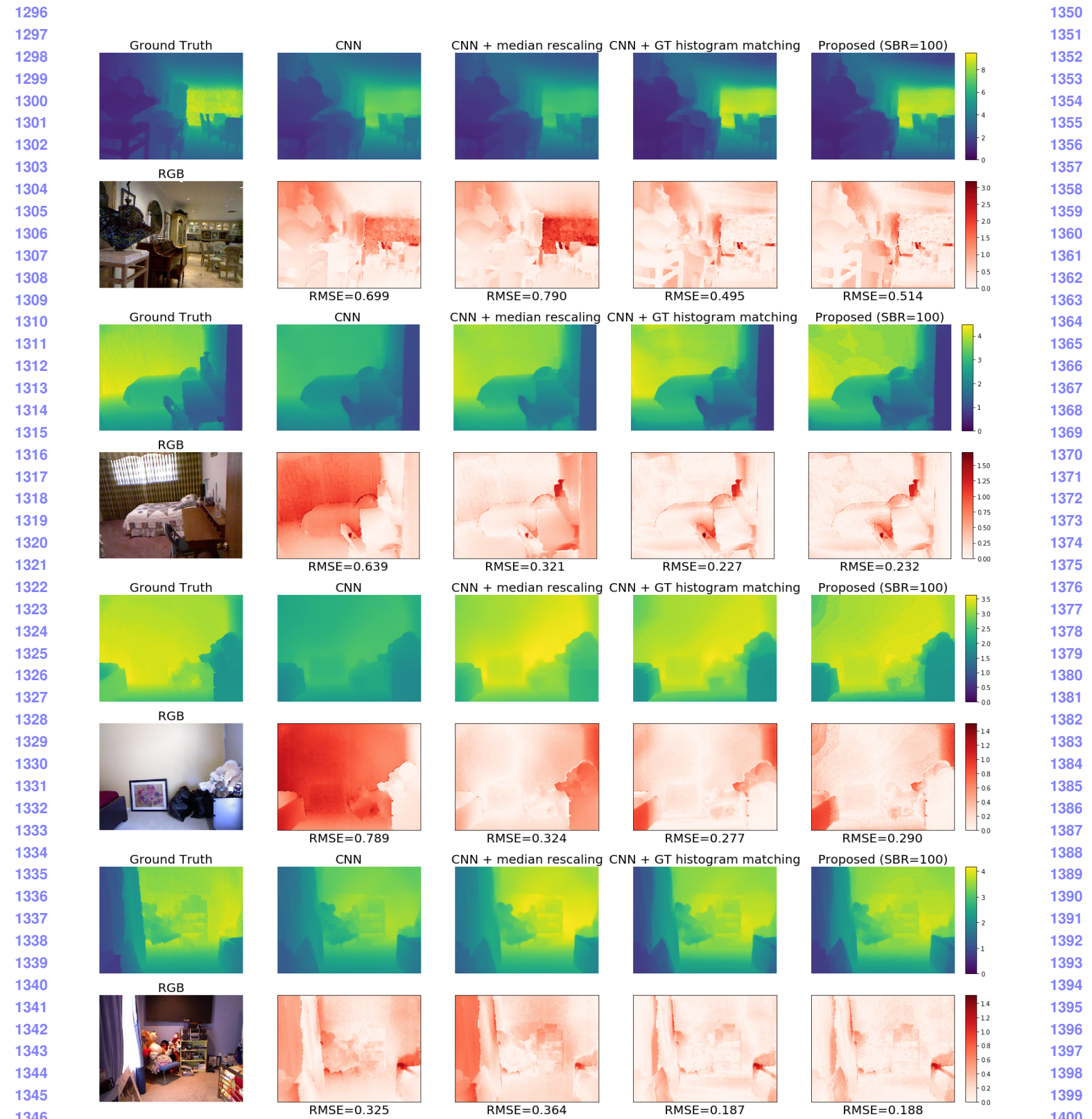


Figure 9: Results on DenseDepth

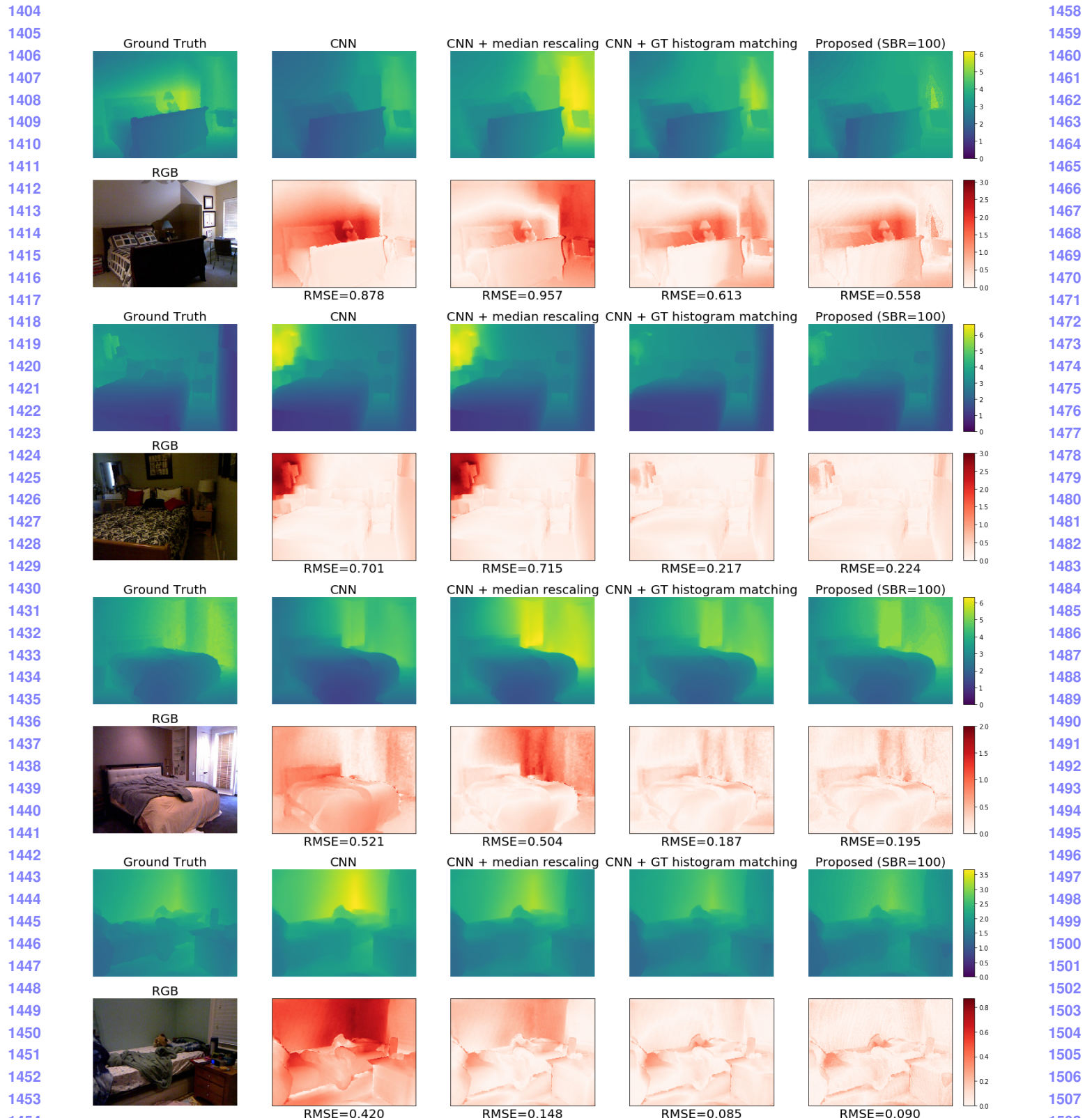


Figure 10: Results on DenseDepth

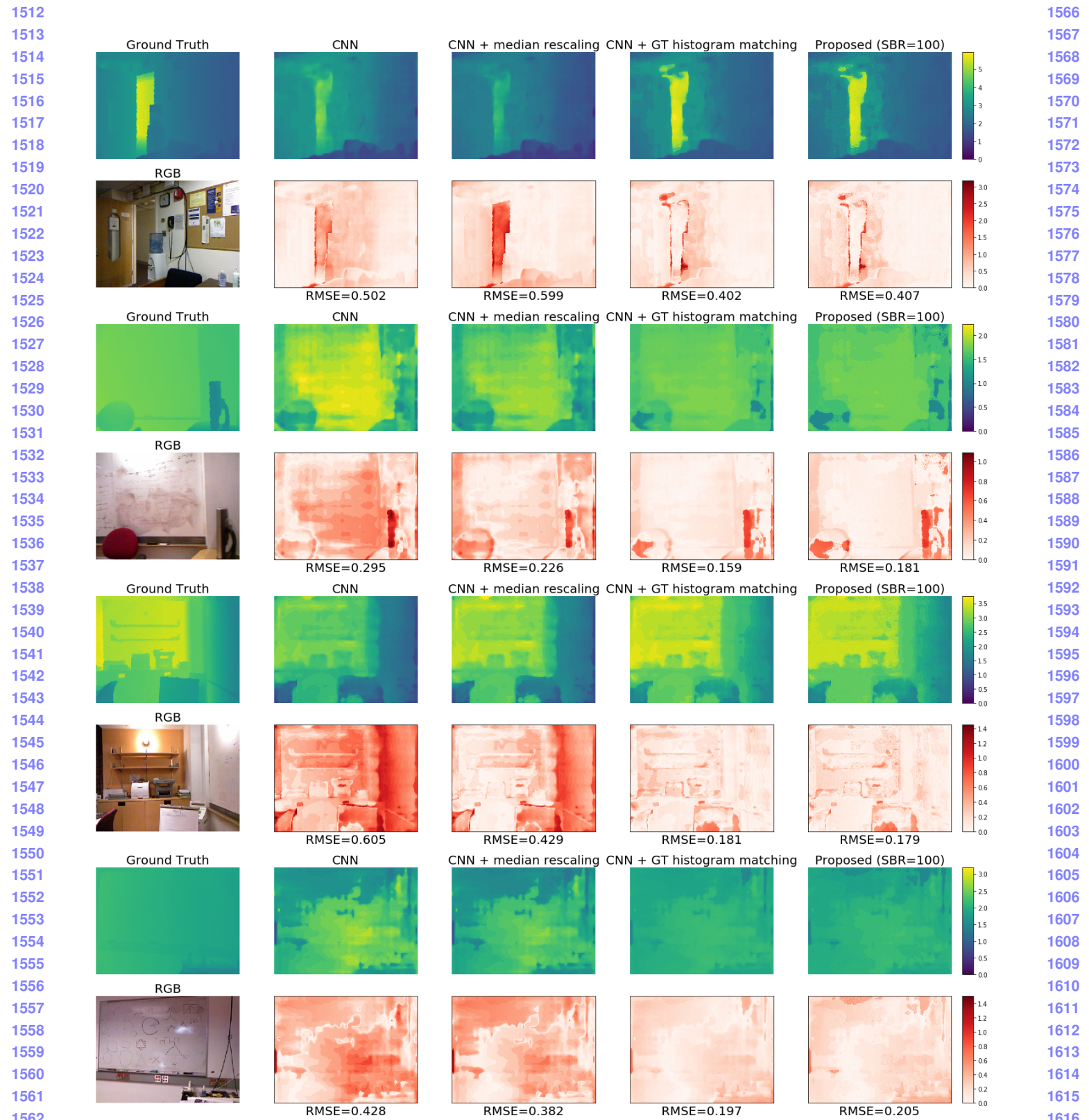


Figure 11: Results on DORN

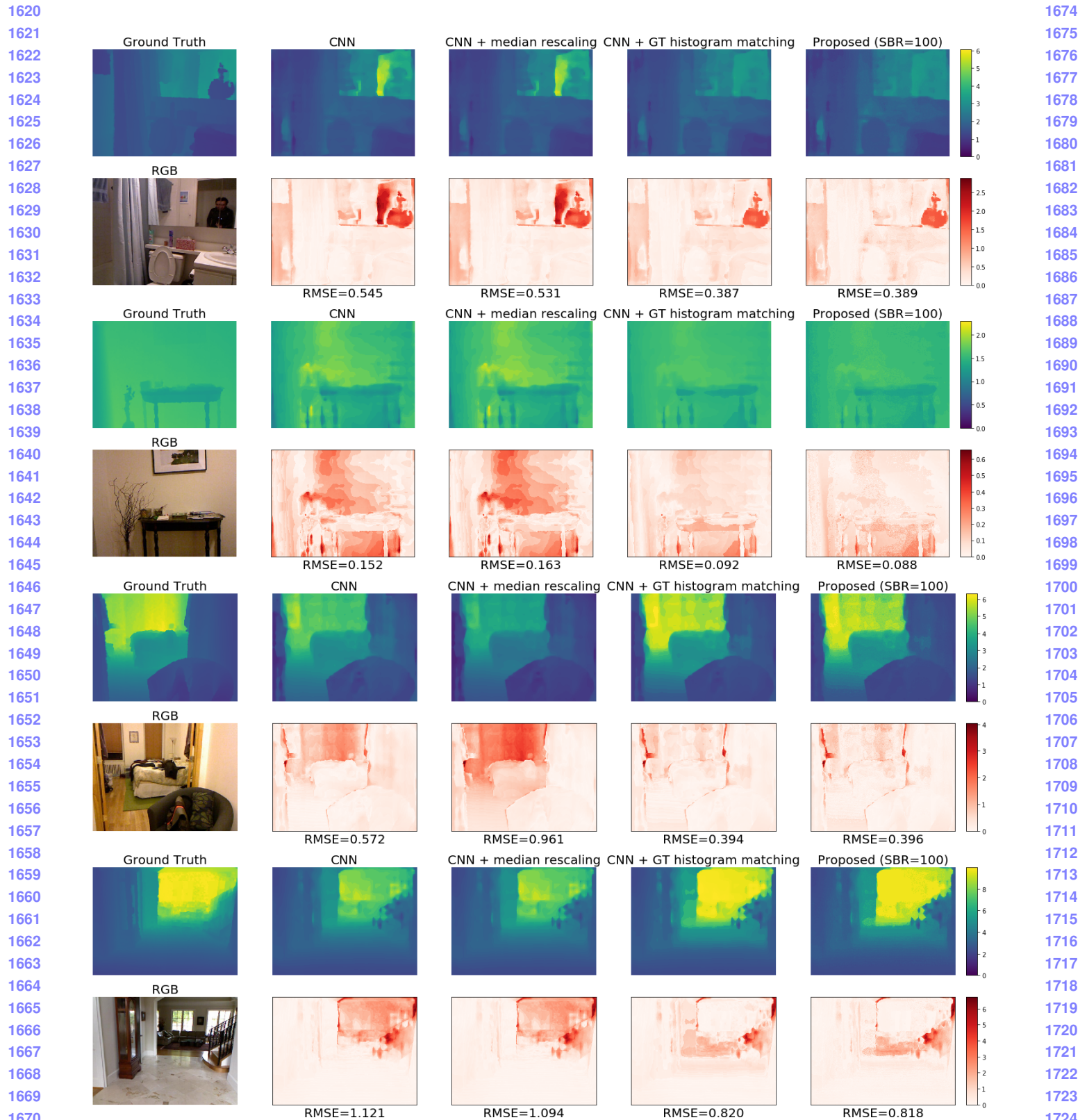


Figure 12: Results on DORN

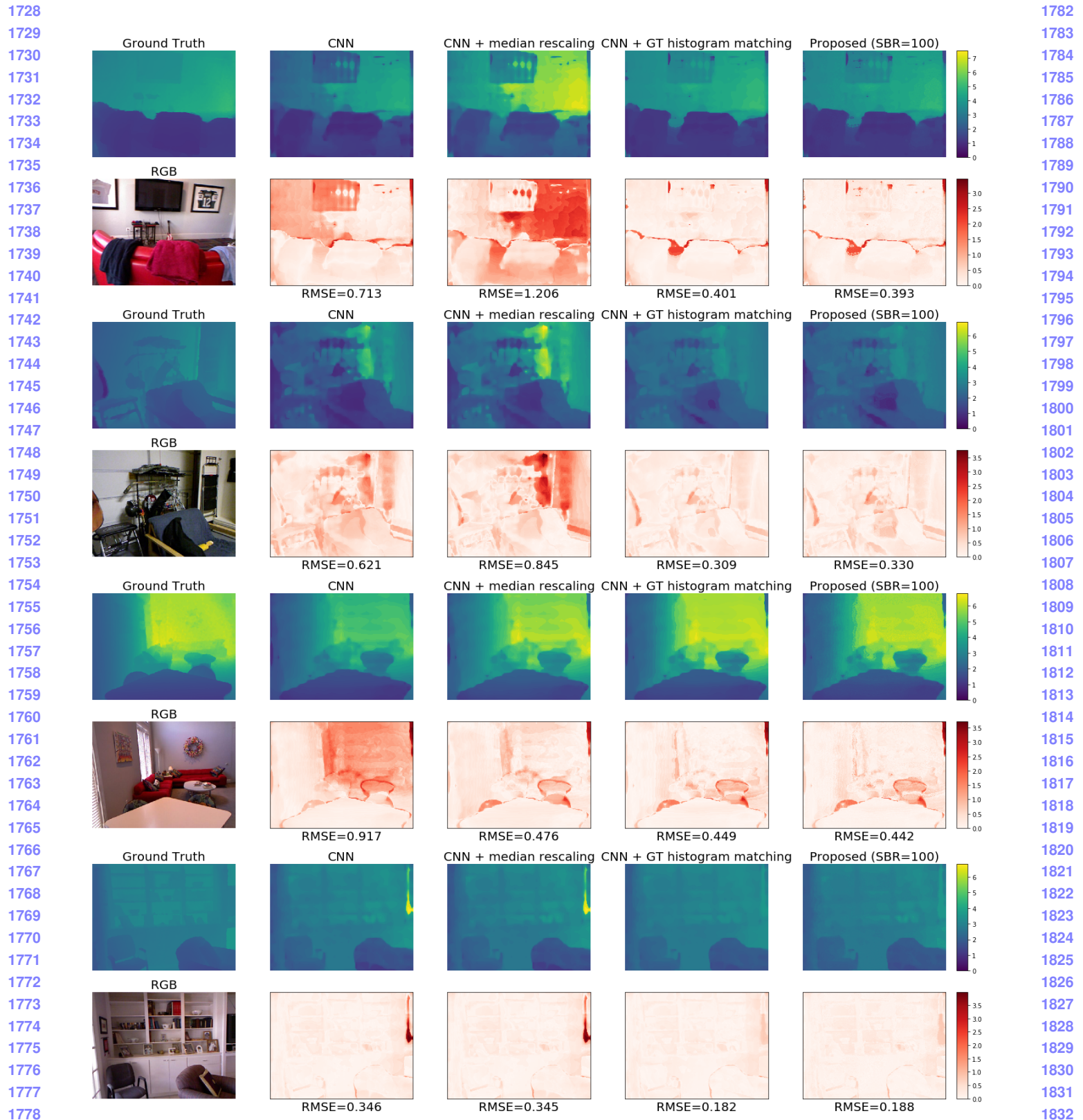


Figure 13: Results on DORN

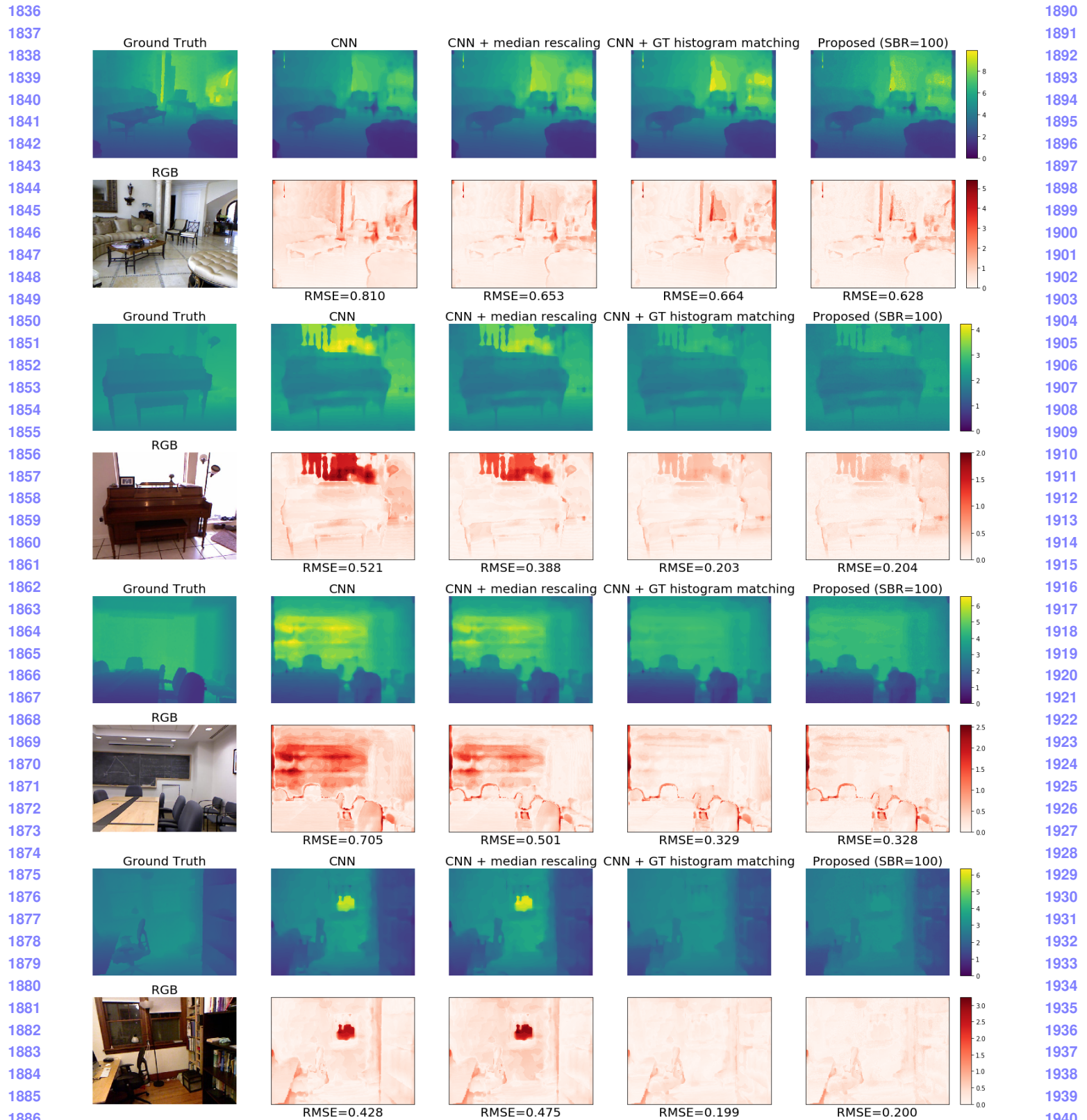


Figure 14: Results on DORN

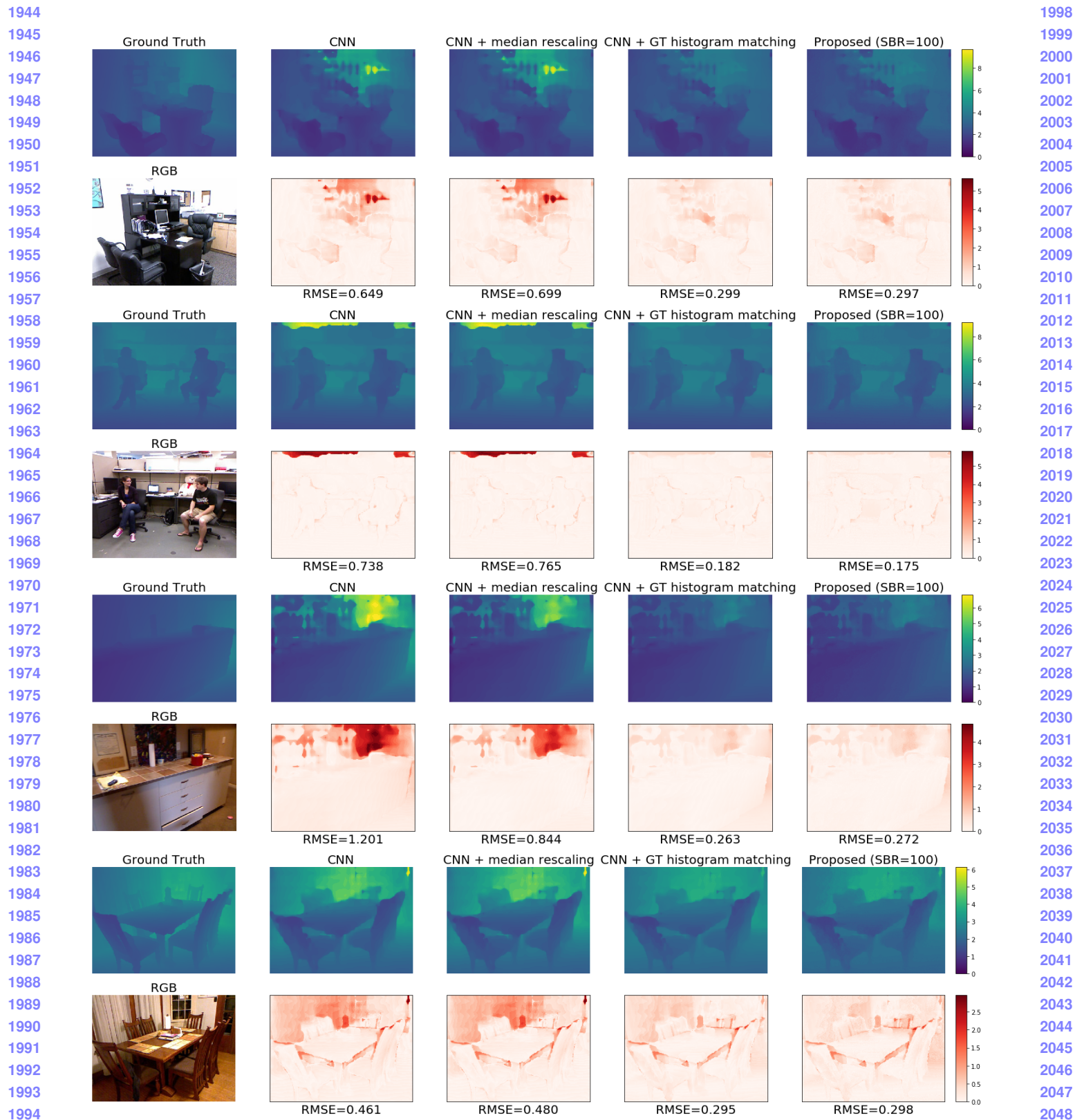


Figure 15: Results on DORN

CVPR
#****

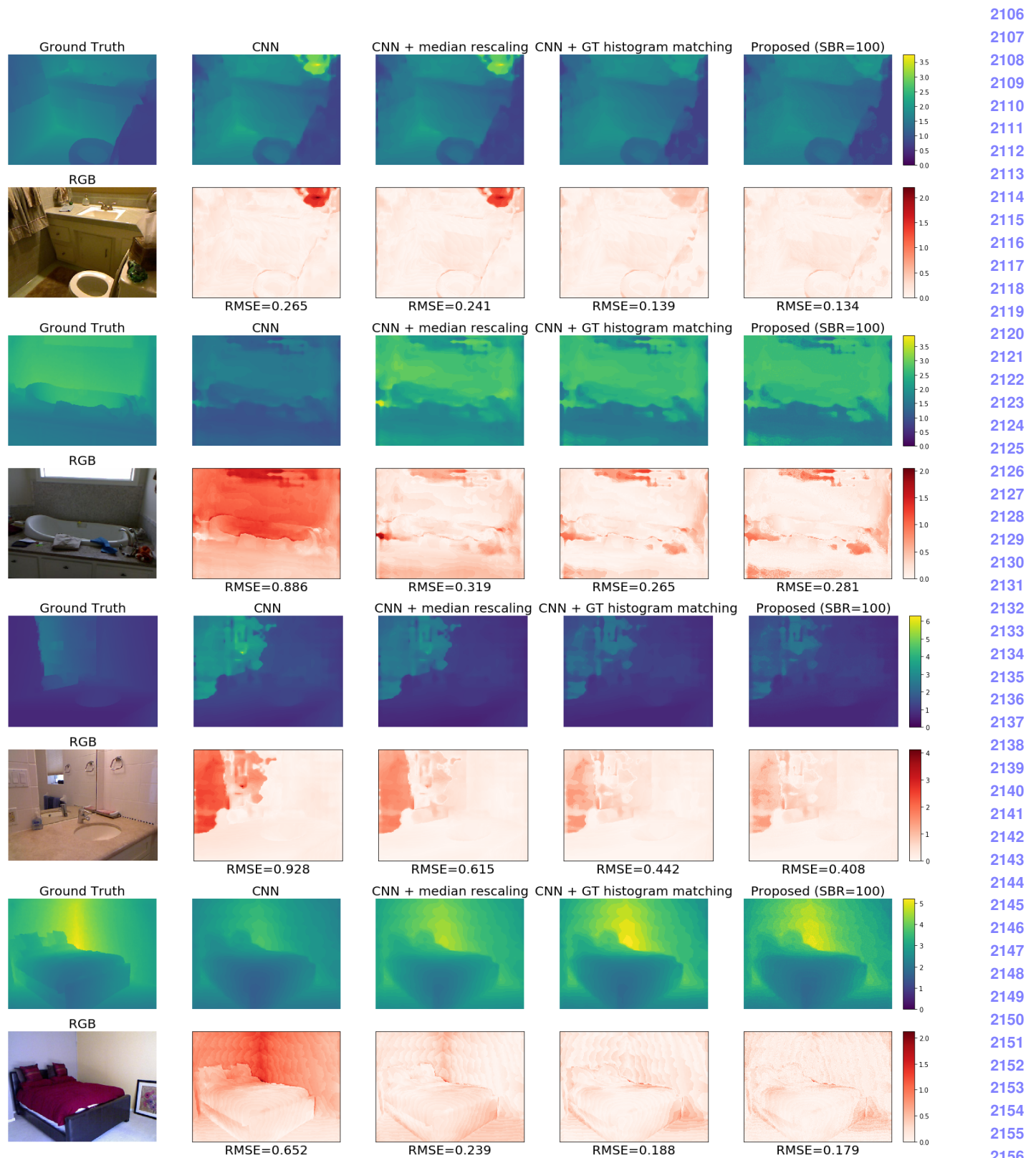
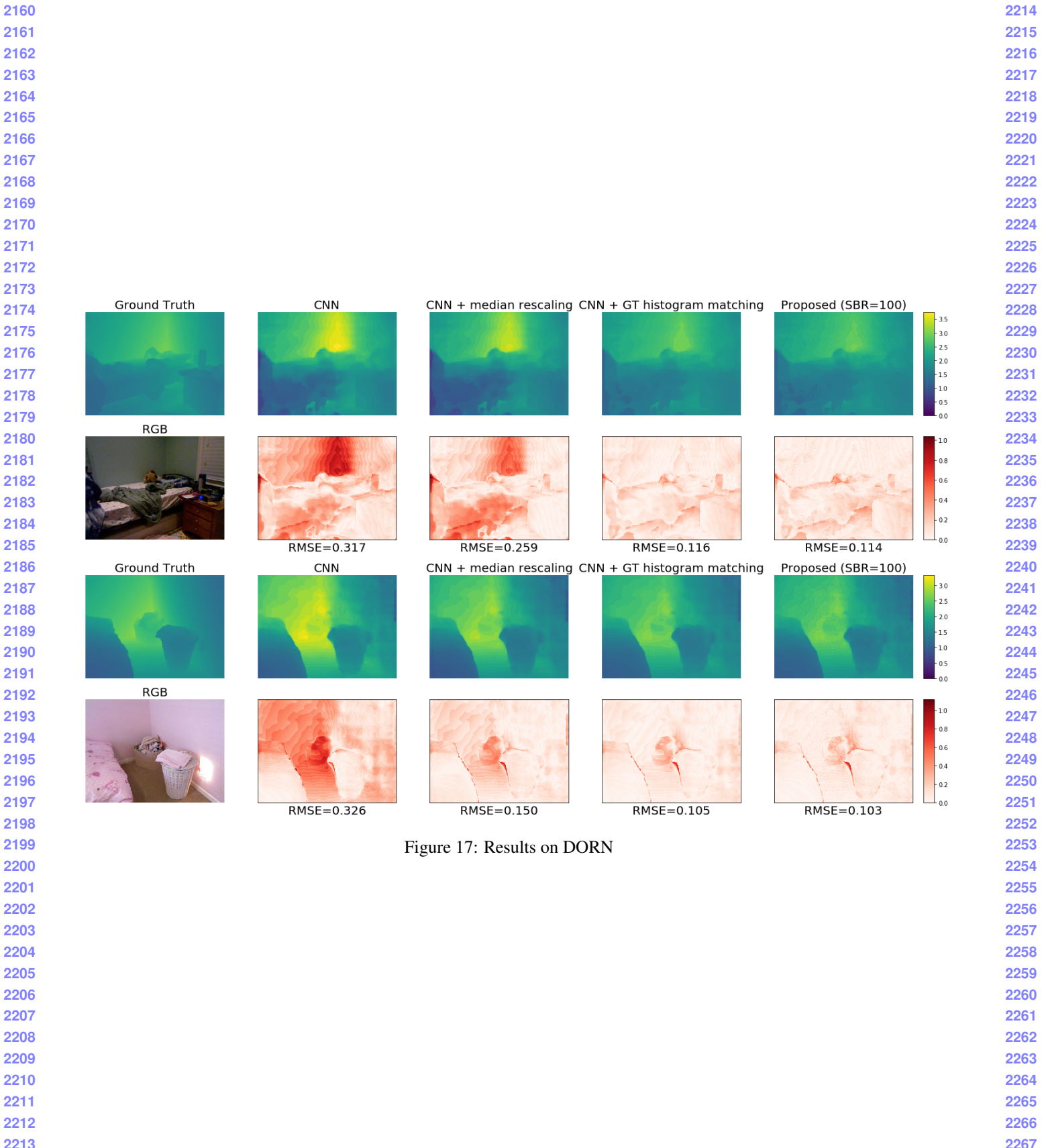
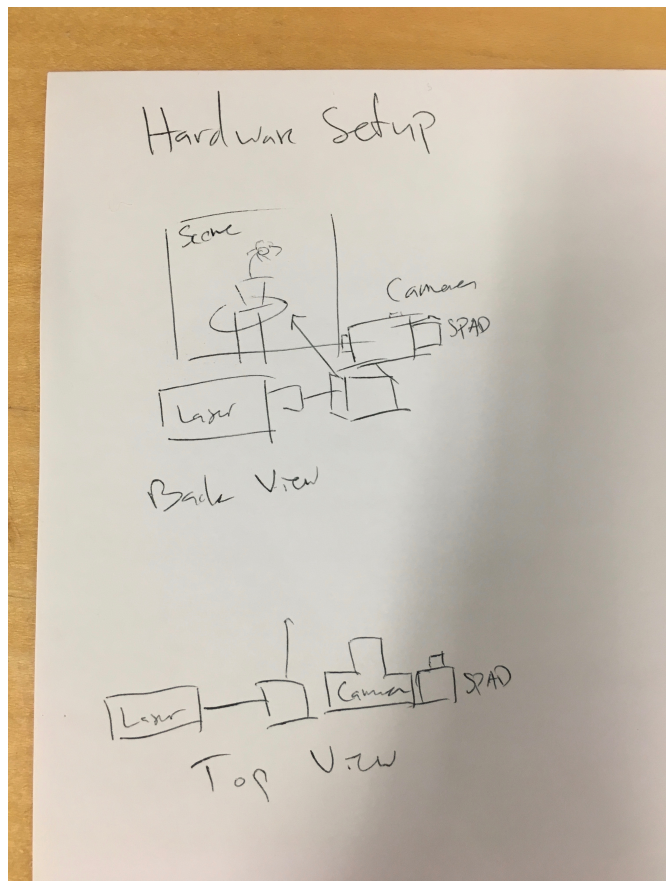


Figure 16: Results on DORN

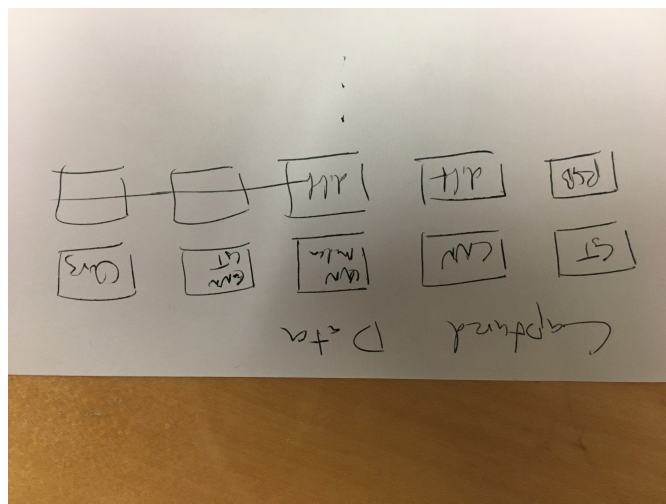


2268
2269
2270
2271
2272
2273
2274
2275
2276
2277
2278
2279
2280
2281
2282
2283
2284
2285
2286
2287
2288
2289
2290
2291
2292
2293
2294
2295
2296
2297

2322
2323
2324
2325
2326
2327
2328
2329
2330
2331
2332
2333
2334
2335
2336
2337
2338
2339
2340
2341
2342
2343
2344
2345
2346
2347
2348
2349
2350
2351
2352
2353
2354
2355
2356
2357
2358
2359
2360
2361
2362
2363
2364
2365
2366
2367
2368
2369
2370
2371
2372
2373
2374
2375

Figure 18: **Hardware setup**

2298
2299
2300
2301
2302
2303
2304
2305
2306
2307
2308
2309
2310
2311
2312
2313
2314
2315
2316
2317
2318
2319
2320
2321

Figure 19: **Hardware results**